JOURNAL OF COMPUTATIONAL PHYSICS **143,** 381–402 (1998)
ARTICLE NO. CP975856

# A Semi-implicit Numerical Scheme for Reacting Flow

## I. Stiff Chemistry

Habib N. Najm,*[,1] Peter S. Wyckoff,* and Omar M. Knio†

**Sandia National Laboratories, P.O. Box 969, MS 9051, Livermore, California 94551, and †Department of Mechanical Engineering, Johns Hopkins University, Baltimore, Maryland 21218-2686*
E-mail: hnnajm@ca.sandia.gov

Received March, 21, 1997; revised August 14, 1997

An additive semi-implicit projection scheme for the simulation of unsteady combustion in two dimensions is constructed. The scheme relies on a zero-Mach number formulation of the compressible conservation equations with detailed chemistry. The governing equations are discretized in space using second-order differences and integrated in time using a semi-implicit approach. Time integration of the evolution equations for species mass fraction, thermodynamic pressure, and density is performed using a semi-implicit, nonsplit scheme that combines a second-order predictor–corrector treatment of convection and diffusion terms, and a stiff integrator for the reaction source terms. Meanwhile, the momentum equations are integrated using a second-order projection scheme. The projection scheme is based on a predictor–corrector approach that couples the evolution of the velocity and density fields in order to stabilize computations of reacting flows with large density variations. A pressure Poisson equation is inverted following both the predictor and corrector steps using a fast solver. The advantages of the stiff integration of reaction source terms are analyzed by comparing the performance of the scheme to that of a predictor–corrector scheme in which reaction and diffusion are integrated in a similar nonstiff fashion. The comparison in based on both one-dimensional (1D) unsteady tests of a premixed methane–air flame, and unsteady two-dimensional tests of the same flame interacting with a counterrotating vortex pair. In both cases, the GRImech1.2 reaction mechanism with 32 species and 177 elementary reactions is used. Computed results show that the stiff reaction scheme enables selection of larger time steps and thus leads to substantial improvement in the performance of the computations. For the present reaction mechanism and flame conditions, speedup factors of about 10 are achieved in the 1D tests and about five in two dimensions.

[1] Corresponding author.



0021-9991/98 $25.00

Possible extensions of the present scheme to further improve efficiency are also discussed. 

*Key Words:* implicit; stiff; chemistry; reacting; flow; projection.

## 1. INTRODUCTION

Direct numerical simulation of turbulent reacting flow is generally difficult, in large part due to the very broad ranges of flow and chemical scales. An immediate consequence of the dynamical flow complexity is that unsteady three-dimensional computation of turbulent combustion with detailed chemistry is beyond the reach of present computational capabilities. Thus, it is essential to consider simplified problems that enable the isolation of representative features of turbulent flames, to develop numerical formulations that efficiently handle the scale disparity of the flow, and to carefully tailor the algorithmic nature of the numerical implementation to optimize the use of available resources. This is the general direction of the present investigation.

It is a well-known fact that incorporation of a detailed chemical kinetic mechanism in a reacting flow model can result in a stiff system of governing equations. As a consequence of this stiffness, explicit time integration of reaction source terms is restricted to very small time steps, leading to inefficient implementations. The severity of this limitation can be illustrated by noting that, for the methane–air reaction mechanism presently considered, the critical time step ($\sim$2 ns) in an explicit scheme is governed by the stiffness of the reaction source term and is substantially smaller than the diffusive stability limit ($\sim$20 ns in 2D for an atmospheric methane–air flame, with a uniform mesh $h = 15.6\,\mu$m). Naturally, restrictions of the same nature also arise in various other applications where stiff reactions prevail.

There has been a considerable amount of work on the numerical integration of stiff systems of ordinary differential equations (ODEs) [1, 2], which arise in a wide range of applications, from combustion to atmospheric modeling, to electrical circuits. It was Curtiss and Hirschfelder [3] who provided the first pragmatic definition of stiff equations as those for which certain implicit methods, particularly backward difference formulas (BDF), perform better than explicit ones. More recently, various stiff ODE-integration code packages, generally based on Gear's [4] variable-order BDF method, have been developed (e.g., GEAR [5], GEARB [6], LSODE [7, 8], and VODE [9]). Particularly, in LSODE and VODE, nonstiff systems are integrated with Adams–Moulton/Adams multistep formulae, whereas stiff systems are integrated using BDFs, which are solved using a modified iterative Newton procedure. A recent review and comparison of various schemes for the integration of stiff chemical kinetic rate equations [10] is presented by Saylor and Ford [11].

It should be emphasized, of course, that the implementation of elaborate stiff schemes such as those in LSODE and VODE involves significant computational overhead. Thus, one concern is whether the advantages achieved by the use of stiff (or implicit) integration schemes, which may enable large stable time steps, are not offset by the additional cost associated with the numerical solution of systems of linear equations. This issue has received renewed attention in the literature, and recent experiences with systems involving detailed reaction mechanisms, including atmospheric chemistry (e.g., [12]) and combustion (e.g., [13, 14]), reveal that despite the additional computational overhead required, stiff schemes remain quite attractive. Furthermore, in light of the computational and theoretical study of D'Angelo and Larrouturou [14], the use of stiff schemes may in fact be highly recommended

for combustion applications with detailed stiff chemistry. Specifically, it is shown in [14] that *some* linearized-implicit schemes and nonstiff fully implicit schemes may be, in practical combustion applications, subject to critical time step restrictions that are more severe than those of fully explicit schemes. Thus, in such situations, careful implementation of a stiff solver may be the best alternative that enables the use of suitably-large, stable time steps.

Several studies aiming at improving the efficiency of stiff integration schemes have recently appeared, the majority of which have specifically focused on reaction mechanisms of the type encountered in atmospheric chemistry. Some of the approaches exploit the special structure of the atmospheric chemistry kinetics which—depending on the mechanism—may lead to sparse Jacobians. This motivates the application of specialized matrix-free inversion techniques (e.g., [15–17]), which in some situations provide an attractive alternative to Newton iterations. When the structure of the equations enables efficient evaluation of higher derivatives, the implementation of stiff, higher order Taylor methods [18] has also been shown to be advantageous.

Other studies have followed a more physically motivated approach, based on the distinction between "slow" and "fast" variables, with long and short characteristic time scales, respectively. In the implementation of such an approach, the evolution equations for the slow variables are typically integrated using explicit formulations, while fast variables are treated using either a stiff Newton-iterative method (e.g., [19, 20]) or "extrapolation" (or "projection") [21, 22] techniques that rely on a quasi-steady-state approximation [23]. The advantage of these approaches is that in the former case, one ends up with a reduced system of implicit nonlinear equations whose solution can be more efficiently performed, while in the latter case an iterative procedure that avoids the inversion of a Jacobian is used. A "hybrid" method [24] has also been proposed, whereby slow variables are integrated with a predictor–corrector formulation while an asymptotic predictor–multicorrector integration is used for the fast variables. Note, however, that sufficient care must be exercised to ensure that the errors associated with these time-scale-segregation schemes are at an acceptable level [11, 12]. When both accuracy and numerical efficiency considerations are included, a recent review [11] finds implicit stiff-integration of the full kinetic equation system to be superior to several schemes that rely on segregation of time scales [23–25]. Other variants of enhanced implementation of stiff schemes include the selective (adaptive) use of stiff and nonstiff methods based, for example, on "time-local" rates of heat release [26]. In these situations, significant savings may be achieved whenever the stiff formulation, and the associated overhead, can be avoided.

Unfortunately, the effectiveness of specialized stiff implementations such as those mentioned above in one- or multidimensional unsteady combustion applications is far from evident. Two issues need to be specifically addressed. The first stems from the fact that in one- or multidimensional reacting flow, the chemical stiffness of the equations is compounded, if not significantly aggravated, by diffusive, convective, and, if relevant, sonic phenomena. This issue is of particular importance for premixed flames, which tend to be characterized by very thin fronts. In these situations, one may expect that diffusion, reaction, and convection are tightly coupled, at least in the neighborhood of the moving flame front. Thus, one concern is whether an operator-split formulation, used typically to reduce the integration of reaction source terms to a zero-dimensional setting, would lead to large integration errors. Recent evidence in this area [14, 27, 28] suggests that operator-split formulations generally tend to penalize the accuracy of integration. The suitability of operator-splitting approaches may thus be problem-dependent and, due in part to rather limited experiences

with unsteady multidimensional reacting flows, is likely to remain an open issue for a while to come. Second, even if an operator-splitting approach is deemed suitable, adaptation of the specialized stiff integrators mentioned above to unsteady combustion applications may still prove difficult. For instance, some approaches assume a special kinetic mechanism structure and may not easily generalize to complex hydrocarbon chemistry. Others are based on clear identification of "fast" and "slow" species. While this segregation of time-scales may be easily done *a priori* in atmospheric computations, it is by no means obvious in combustion, where relative amplitudes of eigenvalues can change drastically across the flame due to the significant changes in temperature and mixture composition across it. Experience in combustion modeling [29] suggests that tabulation of system eigenvalues over the flame thermo-chemical phase space is a viable approach, providing the necessary information for segregation of time scales for the possible range of parameters. On the other hand, the memory requirements necessary for tabulation make this approach impractical for detailed kinetic mechanisms with large numbers of species.

The discussion above reflects yet another difficulty, namely that a straightforward, simultaneous, implicit treatment of diffusion, convection, and reaction terms is also problematic. Briefly, such an approach would lead to very large systems of nonlinear equations, whose solution can be prohibitive due to excessive memory and CPU requirements. Due in large part to these difficulties, it is generally recognized that semi-implicit, mixed formulations are more suitable than fully implicit schemes, at least for unsteady multidimensional applications. These typically combine an implicit or stiff integration procedure for reaction source terms with an explicit treatment of convection and either explicit [14, 27, 30, 31] or implicit [22, 28, 32] treatment of diffusion. Implicit treatment of diffusion appears to be desirable for the simulation of premixed flames which, due to their thin structure are subject to stiff diffusive time-step restrictions. When an operator-split formulation is used, implicit diffusion equations can be efficiently performed, especially when a constant-property model is used. When a nonsplit formulation is used and/or variable mixture properties are accounted for, the use of alternating-direction-implicit (ADI) schemes [22, 32] may be particularly attractive.

This paper describes initial steps towards the construction of an efficient numerical scheme for the direct simulation of unsteady, multidimensional combustion with stiff detailed chemistry. The specific objective of this phase of the effort is to explore the enhancement of a projection scheme for the simulation of unsteady, multidimensional combustion with detailed chemistry by incorporation of a stiff integrator. Attention is focused exclusively on overcoming the temporal stiffness due to the reaction mechanism. Issues related to diffusion stiffness, specialized solvers, and operator-splitting approaches are deliberately omitted from the scope of the present effort. The starting point in the development is the predictor–corrector projection scheme which was developed and tested in previous efforts [33, 34]. As summarized in Section 2, the underlying physical model is based on a zero-Mach-number formulation of the compressible conservation equations (e.g., [34–37]). The zero-Mach-number formulation accounts for the compressibility of the medium but ignores the effect of elastic waves. Thus, it naturally avoids potential sonic CFL limitations. Section 3 provides a brief summary of the nonstiff predictor–corrector projection scheme and describes its extension to stiff chemistry. The extension is based on modifying the corrector step by incorporating a stiff integrator scheme for the reaction source terms. The performance of the stiff code is analyzed in Section 4.1 in light of one-dimensional (1D) unsteady tests on the propagation of a premixed methane–air flame. In particular, the tests

are used to analyze the convergence of the stiff computations and to evaluate the resulting improvement in code performance. The performance of the stiff code is further analyzed in Section 4.2 in light of an extended two-dimensional (2D) simulation of the interaction of a premixed methane–air flame with a counterrotating vortex pair. Conclusions are given in Section 5, which also provides a discussion of the present improvements and motivates further extensions.

## 2. FORMULATION

The physical model is based on a zero-Mach-number formulation of the compressible conservation equations [35]. In the zero-Mach-number limit, acoustic wave propagation is ignored, and the pressure field is decomposed into a spatially uniform component $P_0(t)$ and a hydrodynamic component $p(\mathbf{x}, t)$ which varies both in space and time. Attention is restricted here to open domains; i.e., the thermodynamic pressure $P_0$ is constant in time as well. The present model assumes a two-dimensional flow, zero bulk viscosity [38], and a detailed chemical reaction mechanism that involves $N$ species and $M$ elementary reactions. Soret and Dufour effects [39], radiant heat transfer, and body forces are ignored. The mixture is assumed to obey the perfect gas law, with individual species molecular weights, specific heats, and enthalpies of formation, using Fickian binary mass diffusion. Under these assumptions, the nondimensional mass, momentum, and energy conservation equations are respectively expressed as

$$\frac{\partial \rho}{\partial t} + \nabla \cdot (\rho \mathbf{v}) = 0 \tag{1}$$

$$\frac{\partial(\rho u)}{\partial t} + \frac{\partial(\rho u^2)}{\partial x} + \frac{\partial(\rho u v)}{\partial y} = -\frac{\partial p}{\partial x} + \frac{1}{\mathrm{Re}}\Phi_x \tag{2}$$

$$\frac{\partial(\rho v)}{\partial t} + \frac{\partial(\rho v u)}{\partial x} + \frac{\partial(\rho v^2)}{\partial y} = -\frac{\partial p}{\partial y} + \frac{1}{\mathrm{Re}}\Phi_y \tag{3}$$

$$\frac{\partial T}{\partial t} + \mathbf{v} \cdot \nabla T = \frac{1}{\mathrm{Re\,Pr}} \frac{\nabla \cdot (\lambda \nabla T)}{\rho c_p} + \frac{1}{\mathrm{Re\,Sc}} \frac{\mathbf{Z} \cdot \nabla T}{c_p} + \mathrm{Da} \frac{w_T}{\rho c_p} \tag{4}$$

where $\rho$ is the density, $\mathbf{v} = (u, v)$ is the velocity vector, Re, Pr, Sc, and Da are the Reynolds, Prandtl, Schmidt, and Damköhler numbers respectively, $\Phi_x$, $\Phi_y$ are the viscous stress terms, $\mathbf{Z} \equiv \sum_{i=1}^{N} c_{p,i} D_{iN} \nabla Y_i$, $c_{p,i}$ is the specific heat of the $i$th species at constant pressure, $c_p = \sum_{i=1}^{N} Y_i c_{p,i}$ is the corresponding mixture specific heat, $T$ is the temperature, $\lambda$ is the thermal conductivity, $w_T = -\sum_{i=1}^{N} h_i w_i$ is the chemical heat release source term, $h_i = h_i^o + \int_{T^o}^{T} c_{p,i}\, dT$ is the enthalpy of species $i$, $w_i$ is the production rate of species $i$, and the superscript $o$ is used to denote known reference conditions.

The $N$th species, here $N_2$, is assumed dominant such that the diffusion velocity of any other species $i \neq N$ in the mixture is approximated by $\mathbf{V}_i = -D_{iN} \nabla Y_i / Y_i$, where $D_{iN}$ is the binary mass diffusion coefficient of species $i$ into the $N$th species at the mixture local temperature and stagnation pressure, and $Y_i$ is the mass fraction of species $i$. $\mathbf{V}_N$ is found from the identity $\sum_{i=1}^{N} Y_i \mathbf{V}_i = 0$. Further, for computational efficiency, mixture transport properties $(\mu, \lambda)$ are set to those of the dominant species at the local temperature.

The conservation equation for the $i$th species, $i = 1, \ldots, N-1$, is written as

$$\frac{\partial(\rho Y_i)}{\partial t} = -\nabla \cdot (\rho \mathbf{v} Y_i) + \frac{1}{\mathrm{Re\,Sc}} \nabla \cdot (\rho D_{iN} \nabla Y_i) + Da\, w_i, \tag{5}$$

and the mass fraction $Y_N$ is found from the identity $\sum_{i=1}^{N} Y_i \equiv 1$. The perfect gas state equation is expressed as $P_o = \rho T/\overline{W}$, where $\overline{W} \equiv 1/(\sum_{i=1}^{N} Y_i/W_i)$ is the local effective molar mass of the mixture. The production rate for each species is given by the sum of contributions of elementary reactions [39], with Arrhenius rates $r_k = A_k T^{b_k} e^{-E_k/RT}$, $k = 1, \ldots, M$. The overall progress of an elementary reaction accounts for both forward and backward rates, and corrections for third body efficiencies, and pressure dependence [40].

Finally, for the purposes of the numerical implementation described below, the time rate of change of density is found by differentiating the equation of state,

$$\frac{\partial \rho}{\partial t} = \rho \left( -\frac{1}{T}\frac{\partial T}{\partial t} - \overline{W} \sum_{i=1}^{N} \frac{1}{W_i}\frac{\partial Y_i}{\partial t} \right) \tag{6}$$

and substituting for $\partial T/\partial t$ and $\partial Y_i/\partial t$ from Eqs. (4) and (5), respectively.

## 3. NUMERICAL SOLUTION

As mentioned in the Introduction, the starting point in the construction of the stiff scheme is a second-order predictor–corrector projection scheme [41, 42] for 2D unsteady flow. Below, we first provide a brief description of the original predictor–corrector scheme and then discuss its extension to stiff reactions.

### 3.1. *Predictor–Corrector Projection Scheme*

The predictor–corrector scheme is based on a second-order finite difference discretization of the equations of motion [33, 34]. Specifically, we assume an open 2D rectangular domain, and discretize variables using a staggered grid with uniform cell size in each coordinate direction. Velocity components are specified at cell edges, while scalar fields are discretized at cell centers. Spatial derivatives are approximated using second-order centered differences.

Numerical integration of the semidiscrete equations is performed using a predictor–corrector approach. The predictor uses a second-order Adams–Bashforth time integration scheme to update the velocity and scalar fields and incorporates a pressure correction step in order to satisfy the continuity equation. The corrector relies on a second-order quasi Crank–Nicolson integration, and also incorporates a pressure correction step. In both cases, the pressure correction step involves the inversion of a pressure Poisson equation which is implemented using a fast Poisson solver. Implementation of the algorithm is summarized as follows.

PREDICTOR.

**1.** The local time derivatives $\partial T/\partial t|^n$, $\partial(\rho Y_i)/\partial t|^n$, $i = 1, \ldots, N-1$, and $\partial \rho/\partial t|^n$, are evaluated from Eqs. (4), (5), and (6), respectively.

**2.** Predicted values for the density and scalar concentration fields are determined using

$$\frac{\rho^* - \rho^n}{\Delta t} = \frac{3}{2}\frac{\partial \rho}{\partial t}\bigg|^n - \frac{1}{2}\frac{\partial \rho}{\partial t}\bigg|^{n-1} \tag{7}$$

$$\frac{\rho^* Y_i^* - \rho^n Y_i^n}{\Delta t} = \frac{3}{2}\frac{\partial (\rho Y_i)}{\partial t}\bigg|^n - \frac{1}{2}\frac{\partial (\rho Y_i)}{\partial t}\bigg|^{n-1} \tag{8}$$

and the predicted temperature distribution is found from the equation of state,

$$T^* = P_o \overline{W}^* / \rho^*. \tag{9}$$

**3.** An intermediate velocity field, $\hat{\mathbf{v}} = (\hat{u}, \hat{v})$, is then determined by integrating the pressure-split momentum equations [42],

$$\frac{\rho^* \hat{u} - \rho^n u^n}{\Delta t} = \frac{3}{2} R_x^n - \frac{1}{2} R_x^{n-1} \tag{10}$$

$$\frac{\rho^* \hat{v} - \rho^n v^n}{\Delta t} = \frac{3}{2} R_y^n - \frac{1}{2} R_y^{n-1}, \tag{11}$$

where

$$R_x = -\frac{\partial(\rho u^2)}{\partial x} - \frac{\partial(\rho u v)}{\partial y} + \frac{1}{\mathrm{Re}} \Phi_x \tag{12}$$

$$R_y = -\frac{\partial(\rho v u)}{\partial x} - \frac{\partial(\rho v^2)}{\partial y} + \frac{1}{\mathrm{Re}} \Phi_y. \tag{13}$$

**4.** The intermediate hydrodynamic pressure field is determined by inverting the pressure Poisson equation [43],

$$\nabla^2 p^* = \frac{1}{\Delta t} \left[ \nabla \cdot (\rho^* \hat{\mathbf{v}}) + \left. \frac{\partial \rho}{\partial t} \right|^* \right], \tag{14}$$

where $\partial\rho/\partial t|^*$ is given by the second-order discretization [44]:

$$\left. \frac{\partial \rho}{\partial t} \right|^* = \frac{1}{2\Delta t} (3\rho^* - 4\rho^n + \rho^{n-1}). \tag{15}$$

Note that $\partial\rho/\partial t|^*$ cannot be evaluated directly from Eq. (6) since $(u^*, v^*)$ are not known at this stage.

**5.** Finally, the predicted velocity field $\mathbf{v}^* = (u^*, v^*)$, is obtained using the projection step:

$$\frac{\rho^* u^* - \rho^* \hat{u}}{\Delta t} = -\frac{\partial p^*}{\partial x} \tag{16}$$

$$\frac{\rho^* v^* - \rho^* \hat{v}}{\Delta t} = -\frac{\partial p^*}{\partial y}. \tag{17}$$

CORRECTOR.

**6.** The temporal derivatives of the scalar fields at the new time level $t_{n+1}$ are estimated based on the predicted values, and corrected values for the density and species concentrations are obtained using a second-order quasi Crank–Nicolson integration [45],

$$\frac{\rho^{n+1} - \rho^n}{\Delta t} = \frac{1}{2} \left( \left. \frac{\partial \rho}{\partial t} \right|^n + \left. \frac{\partial \rho}{\partial t} \right|^{**} \right) \tag{18}$$

$$\frac{\rho^{n+1} Y_i^{n+1} - \rho^n Y_i^n}{\Delta t} = \frac{1}{2} \left( \left. \frac{\partial(\rho Y_i)}{\partial t} \right|^n + \left. \frac{\partial(\rho Y_i)}{\partial t} \right|^{**} \right) \tag{19}$$

while the new temperature distribution is found using the equation of state,

$$T^{n+1} = P_o \overline{W}^{n+1} / \rho^{n+1}. \tag{20}$$

The estimates for $\partial T/\partial t|^{**}$, $\partial(\rho Y_i)/\partial t|^{**}$, and $\partial\rho/\partial t|^{**}$ are obtained by substituting the predicted scalar and velocity fields into Eqs. (4), (5), and (6), respectively.

**7.** A second, intermediate velocity field $\mathbf{v}' = (u', v')$ is determined using the pressure-split momentum equations:

$$\frac{\rho^{n+1}u' - \rho^n u^n}{\Delta t} = \frac{3}{2}R_x^n - \frac{1}{2}R_x^{n-1} \tag{21}$$

$$\frac{\rho^{n+1}v' - \rho^n v^n}{\Delta t} = \frac{3}{2}R_y^n - \frac{1}{2}R_y^{n-1}. \tag{22}$$

**8.** The pressure distribution at the new time level is obtained by inverting the pressure Poisson equation,

$$\nabla^2 p^{n+1} = \frac{1}{\Delta t}\left[\nabla\cdot(\rho^{n+1}\mathbf{v}') + \left.\frac{\partial\rho}{\partial t}\right|^{n+1}\right] \tag{22}$$

with

$$\left.\frac{\partial\rho}{\partial t}\right|^{n+1} = \frac{1}{2\Delta t}(3\rho^{n+1} - 4\rho^n + \rho^{n-1}). \tag{23}$$

Here again, $\partial\rho/\partial t|^{n+1}$ cannot be evaluated directly from Eq. (6) since $(u^{n+1}, v^{n+1})$ are not known at this point.

**9.** Finally, the velocity field at the new time level $\mathbf{v}^{n+1} = (u^{n+1}, v^{n+1})$ is determined using

$$\frac{\rho^{n+1}u^{n+1} - \rho^{n+1}u'}{\Delta t} = -\frac{\partial p^{n+1}}{\partial x} \tag{24}$$

$$\frac{\rho^{n+1}v^{n+1} - \rho^{n+1}v'}{\Delta t} = -\frac{\partial p^{n+1}}{\partial y}. \tag{25}$$

The above predictor–corrector scheme has been used in [33] for reacting flow modeling. Tests have shown that the predictor alone is conditionally stable for relatively low ratios between the temperature of the burnt ($T_b$) and unburnt ($T_u$) fluids, roughly $T_b/T_u \leq 2$. At higher temperature ratios, incorporation of the corrector step is necessary for stability.

Finally, we note that the present scheme has common aspects with several earlier computational studies of chemically reacting flows at low Mach number, in particular those of McMurtry *et al.* [43], Rutland *et al.* [46, 47], and Mahalingam *et al.* [44]. The present formulation resembles more closely that of Rutland *et al.*, who also used a predicator–corrector approach.

### 3.2. *Projection Scheme for Stiff Chemistry*

Extension of the above scheme to stiff chemistry is based on modifying the update of the scalar fields in the corrector step only. Thus, the predictor step is left unchanged, and

the velocity update in the corrector step is performed in an identical fashion as in the original scheme summarized above. In the stiff scheme, the scalar update in the corrector step is based on a mixed, nonsplit (additive) integration of the species and density evolution equations. Consequently, all the terms which explicitly involve the species rate equations are handled using a stiff integrator which is adapted from the DVODE integration package [9]. Meanwhile, all the remaining terms are treated as in the original formulation, i.e. using a quasi Crank–Nicolson approach.

In order to describe the construction of the stiff corrector, we first rewrite the species and density evolution equations in a form suitable for a mixed semi-implicit additive stiff integration. Specifically, the species mass fraction evolution equation is written as

$$\frac{\partial(\rho Y_i)}{\partial t} = C_i + D_i + R_i, \tag{26}$$

where

$$C_i = C_i(\rho, \mathbf{v}, Y_i) \equiv -\nabla \cdot (\rho \mathbf{v} Y_i) \tag{27}$$

$$D_i = D_i(\rho, T, Y_i) \equiv -\frac{1}{\mathrm{Re\,Sc}} \nabla \cdot (\rho Y_i \mathbf{V}_i) \tag{28}$$

$$R_i = R_i(\rho, T, Y_i) \equiv \mathrm{Da}\, w_i \tag{29}$$

denote the species convection, diffusion, and reaction source terms, respectively. Meanwhile, the density evolution equation is expressed as

$$\frac{\partial \rho}{\partial t} = C_\rho + D_\rho + E_\rho + R_\rho + \mathcal{E}_\rho \tag{30}$$

where

$$C_\rho \equiv \frac{\rho}{T}\left(\mathbf{v} + \frac{1}{c_p \mathrm{Re\,Sc}}\mathbf{Z}\right) \cdot \nabla T \tag{31}$$

$$D_\rho \equiv -\frac{1}{\mathrm{Re\,Pr}\, c_p T} \nabla \cdot (\lambda \nabla T) \tag{32}$$

$$E_\rho \equiv \frac{\overline{W}}{\rho} \sum_{i=1}^{N} \frac{-\nabla \cdot (\rho \mathbf{v} Y_i) - (1/\mathrm{Re\,Sc}) \nabla \cdot (\rho Y_i \mathbf{V}_i) + Y_i \nabla \cdot (\rho \mathbf{v})}{W_i} \tag{33}$$

$$R_\rho \equiv -\frac{1}{c_p T} \mathrm{Da}\, w_T \tag{34}$$

$$\mathcal{E}_\rho \equiv \overline{W} \sum_{i=1}^{N} \frac{\mathrm{Da}\, w_i}{W_i}. \tag{35}$$

Here, $C_\rho$ represents the density source term due to convection and species diffusion, $D_\rho$ the contribution of thermal diffusion, while $R_\rho$ is the reaction source. $E_\rho$ and $\mathcal{E}_\rho$ arise from differentiation of the equation of state and represent the density changes due to the changes in the local mass of the mixture.

The construction of the stiff scheme is based on identifying $R_i$, $R_\rho$, and $\mathcal{E}_\rho$ as stiff terms and treating the remaining terms as in the original formulation. To this end, Eqs. (26)

and (30) are rewritten as a collection of spatially decoupled initial value problems, each consisting of $N$ coupled nonlinear ODEs:

$$\frac{\partial(\rho Y_i)}{\partial t} = \frac{1}{2}\left(C_i^n + D_i^n\right) + \frac{1}{2}\left(C_i^* + D_i^*\right) + R_i(\rho, \rho\mathbf{Y}), \tag{36}$$

$i = 1, \ldots, N-1$, and

$$\frac{\partial \rho}{\partial t} = \frac{1}{2}\left(C_\rho^n + D_\rho^n + E_\rho^n\right) + \frac{1}{2}\left(C_\rho^* + D_\rho^* + E_\rho^*\right) + R_\rho(\rho, \rho\mathbf{Y}) + \mathcal{E}_\rho(\rho, \rho\mathbf{Y}), \tag{37}$$

where $\rho\mathbf{Y} = (\rho Y_1, \rho Y_2, \ldots, \rho Y_{N-1})$ is the reduced local vector of the mass concentrations of all but the last species. Equations (36) and (37) are integrated locally from $t_n$ to $t_{n+1}$ using the DVODE stiff integration routine. The integrations are performed independently at the cell centers, where the scalar fields are defined.

The implementation of the stiff scheme relies on the use of the above two equations in the corrector stage above. The predictor–corrector setup remains unchanged except that $\rho^{n+1}$ and $Y_i^{n+1}$ are found from the stiff-integration procedure applied to Eqs. (36), (37) rather than the quasi Crank–Nicolson formulation in Eqs. (18), (19). Here then is the additional computational overhead required by the stiff scheme. The integration of these two equations may require several evaluations of the reaction rate terms and the Jacobian matrix of the system. Minimizing this overhead is crucial to the performance of the scheme. This necessitates the optimal use of the DVODE integration package.

The integration algorithm in DVODE is based on high-order backward difference formulas, whose implementation requires the solution of a system of nonlinear equations. To this end, DVODE incorporates an iterative nonlinear equation solver. This solver requires an estimate of the Jacobian of the source terms in the original system of ODEs. In the calculations, the Jacobian is evaluated using exact formulas which are derived by analytically differentiating the definitions of $R_i$, $R_\rho$, and $\mathcal{E}_\rho$, given in Eqs. (29), (34), and (35), respectively. As the expressions for the reaction source terms are quite involved [40], the derivation is quite lengthy and leads to a large number of formulas. These are incorporated in the computations but, for brevity, are not reproduced here.

### 3.3. *Computational Issues*

Significant code optimization is necessary to allow efficient modeling of reacting flow with detailed kinetics. This optimization and the performance numbers reported below are based on the available hardware, namely a shared-memory parallel SGI PowerChallenge-L machine with eight R10K processors, and 1 MB secondary cache size. The code is optimized at various levels for both the stiff and nonstiff schemes.

To begin, consider the core reaction rate routine, which is used in both the stiff and nonstiff schemes. As would be expected, this is the most computationally intensive part of the nonstiff scheme. Contrary to initial expectations, however, it is not necessarily the exponential or other intrinsic function evaluations in the reaction rate expressions that are the most expensive. Rather, and depending on computational hardware, memory access operations may be more costly. Particularly, nonsequential array indexing can entail significant memory access overhead, depending on CPU cache size and configuration. In order to minimize this overhead, the reaction rate routine is symbolically generated before the simulation by parsing the specific chemical mechanism of interest. The output is a set of source code files which

are then compiled into the code, eliminating the many looping and indexing constructs which would otherwise be necessary to compute the reaction rates during execution. This technique is also employed in the stiff scheme for both function and jacobian evaluations.

Moreover, the particular data structure implementation has significant implications to parallelization, even on a shared memory architecture. Particularly, in order to enhance the parallel efficiency of the stiff code, the entire stiff integration operation on each cell was designed to be local to the processor owning that cell. This necessitated the modification of the structure of DVODE to use only local data passed through argument lists rather than the original FORTRAN COMMON constructs.

Finally, the present adaptation of DVODE differs from its "normal" application mode which attempts to adaptively optimize the integration time step and accordingly modify the order of integration. To do so, DVODE would require a large amount of memory, which is in large part dominated by storage requirements for previously computed Jacobians. While storage of the Jacobians is possible for small problems, for instance in one spatial dimension, it is generally prohibitive for multidimensional problems with detailed chemistry, except possibly on large massively parallel architectures. To avoid excessive memory requirements, we have opted not to store the Jacobians and to restrict the use of DVODE to a "startup" mode only. While this approach provides a simple means to avoid a severe memory problem, it leads to a suboptimal use of the capabilities of the routine. Nonetheless, as shown in the following section, the present stiff scheme still yields significant computational savings over its predecessor.

## 4. RESULTS

We will study the performance of the above scheme in one- and two-dimensional unsteady flow. We use the GRImech1.2 [48] $C_{(1)}C_{(2)}$ chemical mechanism for premixed methane–air combustion and consider a stoichiometric 20% $N_2$-diluted methane–air flame at atmospheric pressure with reactants at ambient temperature in an open domain. The mole fraction composition of the reactants mixture ($CH_4 : O_2 : N_2$) is (0.08 : 0.15 : 0.77).

### 4.1. *One-Dimensional Flow*

The performance of the stiff scheme is studied in 1D relative to the original nonstiff scheme. An initial condition is computed using Chemkin [40, 49] in 1D for a freely propagating premixed methane–air flame with the above reactants mixture and chemical mechanism. This solution is interpolated onto the uniform 1D grid used in the present code and used to initialize the computations.

The initial flame structure is shown in Fig. 1. The computational domain is 0.8 cm long with outflow boundary conditions. Reactants, products, and key active radical mole fractions are shown. The flame is burning to the left into the reactants. The temperature profile is shown, with the temperature rising from 300 to 1900 K in the flame.

For conciseness let us refer to the nonstiff and stiff schemes as A and B, respectively. Four grid refinement levels are chosen, with $n = 256, 512, 1024$, and 2048 cells on the 1D domain. Given the stiff chemical mechanism under consideration, the time step stability restriction for scheme A is dictated by chemical stiffness and is therefore independent of the cell size $h$ in the range considered. The necessary stable time step for this scheme, determined empirically, is $\Delta t_{c,A} \sim 2$ ns. On the other hand, in the stiff scheme, implicit handling of the chemical source terms using DVODE eliminates this chemical stiffness

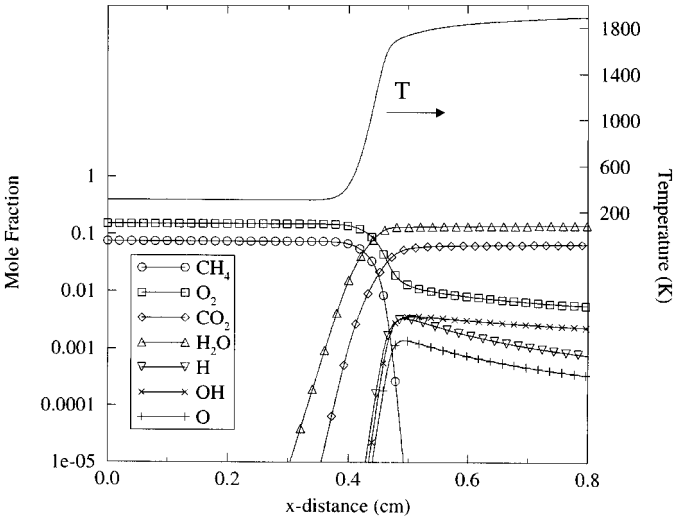


**FIG. 1.** Initial condition corresponding to the 1D premixed methane–air flame, showing mole fractions of reactants, products, and key radicals, as well as the temperature profile.

restriction. Practical experience with the scheme suggests that the time step is then limited by the diffusive stability restriction. Notably, we find that the stiff-integration process in DVODE attempts time steps much larger than the actual time step for which the overall scheme is stable, suggesting that the limitation on the time step is not chemical. Given the maximum diffusivity, $D_{\max}$, namely that of the H radical, and the particular cell size $h$, the classical diffusive stability restriction for an explicit scheme is $D_{\max}\Delta t/h^2 < 1/2^q$, where $q$ is the number of space dimensions. This is in fact the scaling we observe empirically here for $q = (1, 2)$, suggesting that this diffusive stability restriction indeed holds for the present stiff scheme consistent with its semi-implicit construction which uses an explicit/predictor–corrector diffusion formulation.

For the present 1D flow, the critical time step is found to be $\Delta t_{c,B} \sim 40$ ns for $n = 512$ (cell size $h = 15.6\,\mu$m). This spatial resolution is the minimum necessary for adequate representation of the atmospheric premixed methane–air flame structure and is the value used below in the 2D computations. Clearly, the utility of the stiff scheme is evident at this refinement level, with a factor of 20 increase in the time step. Note, however, that implementation of the stiff scheme necessitates additional computational overhead, such that the net speedup factor is smaller than the ratio of time steps. Experience with the scheme indicates that the additional overhead is primarily associated with evaluation of the Jacobian and its inversion, rather than function evaluations. The choice of stiff-integrator relative and absolute tolerances has a relatively small effect on integration cost. For relative and absolute tolerances of $(10^{-6}, 10^{-6})$, the Jacobian is computed once, and the reaction terms are computed three times—once in the predictor and twice in the corrector—per time step per cell. As tolerances are made more stringent, the number of function calls required increase mostly for the few cells within the flame structure, and to a lesser extent in the products behind the flame, but not in the reactants. No additional Jacobian evaluations are necessary anywhere, such that the net result is a minor effect on overall performance. For example, taking the relative and absolute tolerances from $(10^{-6}, 10^{-6})$ to $(10^{-8}, 10^{-12})$ results in a mere 8% increase in CPU time. In the present 1D computations, we measure

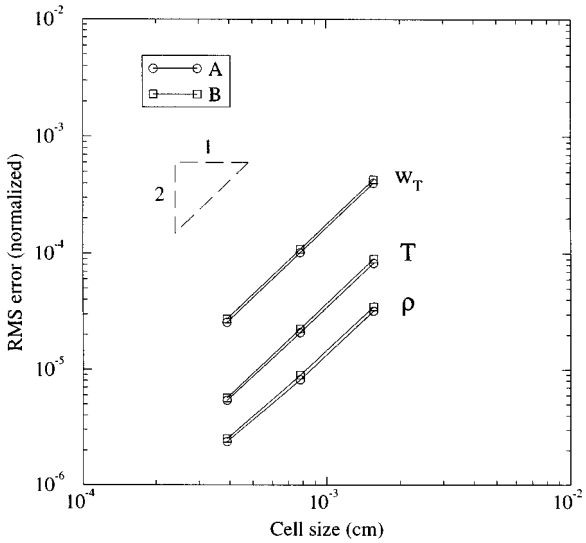


**FIG. 2.** Convergence of the RMS error between 1D flame solutions with successive mesh refinements, for each of the nonstiff (A) and stiff (B) schemes.

a net speedup factor of about 10. Thus, the implementation of the stiff scheme and the associated increase in code complexity are well justified. This advantage vanishes at higher mesh refinement as the diffusive stability limit becomes more restrictive. Thus, for $n = 2048$, $h = 3.9\,\mu m$, $\Delta t_{c,B} \sim 2.5$ ns, and given $\Delta t_{c,A} \sim 2$ ns, results in a "speedup" factor of $\frac{1}{2}(\Delta t_{c,B}/\Delta t_{c,A}) = 0.63$, indicating that the nonstiff scheme is in fact more efficient.

The spatial convergence of the scheme is studied in 1D by comparing the solutions with successive mesh refinement after integration to 0.2 ms. Let $\phi$ be a general field quantity, and $\epsilon$ a root-mean-square (rms) error measure. For each of the two schemes (A or B) we evaluate the relative spatial convergence rate based on $\epsilon^{(h)} = \|\phi^{(h)} - \phi^{(h/2)}\|_2$, where $h$ is the cell size. The time step for the nonstiff scheme is fixed at $\Delta t_A = 2$ ns, while $\Delta t_B \propto h^2$ per the diffusion stability constraint. The corresponding second-order convergence rate for each scheme is illustrated in Fig. 2, using the temperature, density, and heat release rate fields. We also study the rms deviation between the two schemes, which is found to exhibit second-order convergence with $h$ as well, thus demonstrating that the two schemes converge to the same solution. The temporal convergence rate is studied similarly using time-step refinement for a fixed $h$ corresponding to $n = 256$. This study used a precomputed initial condition that provides the necessary second-order startup for the scheme, with a variable time-step version of the Adams–Bashforth procedure used for the first time step. With $\Delta t = 10, 5$, and 2.5 ns, the convergence rates for $T$, $\rho$, and $w_T$ are found to be: 2.2, 2.8, and 1.9, respectively.

### 4.2. *Two-Dimensional Flow*

In a two-dimensional flow we study the interaction of the above premixed methane–air flame with a counterrotating vortex pair. This is a typical flow that has been investigated both numerically [34, 46, 50–53] and experimentally [54–59] and serves as a useful test problem for comparing computed results with published data and for comparisons between the present nonstiff and stiff schemes.

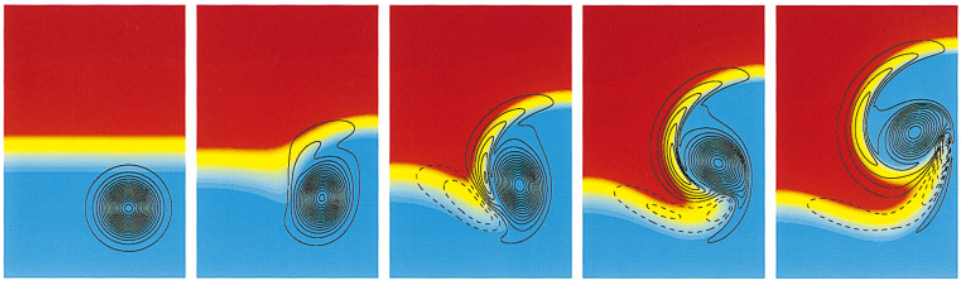

**FIG. 3.** Time sequence illustrating computed flame interaction with the counterrotating vortex-pair, using $0.4 \times 0.6$ cm$^2$ frames. The vertical right-hand side edge of each frame is the centerline of the vortex-pair, only half of which is computed. The time span is from 0 to 0.32 ms, left to right, with an interval between adjacent frames of 0.08 ms. The color map indicates gas temperature, with the unburnt reactants at room temperature in blue, and the burnt combustion products in red. The flame location is roughly where the rapid color transition is observed. The solid/dashed contours delineate levels of positive/negative vorticity, where positive vorticity corresponds to counterclockwise fluid rotation.

An open rectangular domain is considered, with dimensions $0.4 \times 0.8$ cm$^2$, and is overlaid by a $256 \times 512$ grid with uniform cell size in each coordinate direction. We apply symmetry boundary conditions in the horizontal $x$-direction and outflow boundary conditions in the $y$-direction. The initial vorticity and temperature fields at $t = 0$ are shown in the leftmost frame of Fig. 3. The vertical right edge of the domain is the centerline of the vortex pair under consideration, which is one member of an infinite periodic row of vortex pairs along the horizontal $x$-direction. The initial condition is a superposition of the velocity $(u, v)$ field induced by the periodic row of vortex pairs, and the temperature, density, and mass fraction $(T, \rho, Y_i)$ distributions corresponding to a horizontal premixed flame, with the initial structure in the $y$-direction from the above 1D flame shown in Fig. 1. The vorticity field corresponding to each initial vortex is a second-order Gaussian. The initial self-induced velocity of the vortex pair is 300 cm/s. The maximum rotational velocity in the domain is around 20 m/s, giving a Mach number of 0.067, a small value as required by the present formulation.

The results shown in Fig. 3 are computed using the stiff scheme, with a near-critical $\Delta t = 20$ ns. The flame is observed to propagate downward, in the negative $y$-direction, by burning into the reactants. The vorticity field causes significant contortion and large variations in the topology of the flame as the vortex pair propagates upwards into it. A baroclinic vorticity dipole is generated in the neighborhood of the original vortex, in agreement with the numerical results of [33, 46, 50] and the experimental measurements of Mueller *et al.* [59]. This vortical fluid is then entrained into the vortex pair, in a continuing process that leads to the generation of multiple folds of counterrotating vorticity inside the original vortex. By this process some hot products are entrained into the reactants in the vortex core, enhancing the ongoing diffusive heating of the cold unburnt fluid in the core. The global dynamics of this flow involve rapid penetration of the fast vortex pair into the flame and the formation of a pocket of unburnt material carried through by the vortex pair. These dynamics reflect the relative disparity between flame and vortex-pair time scales, the ratio of which yields a Damköhler number $Da = 0.04$. With $Da \ll 1$, the flow is significantly faster than the flame, and it is expected that significant contortion of the flame will occur, as observed here. In a turbulent flow regime, this would correspond to a well-stirred condition [60].

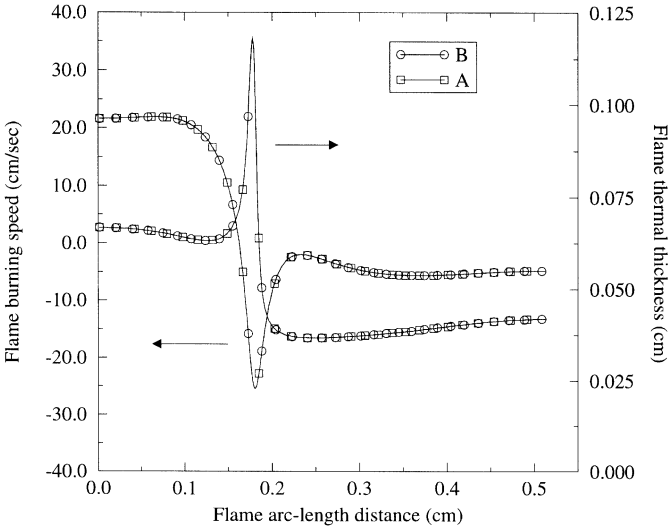


**FIG. 4.** Flame laminar burning speed (relative to the unburnt fluid) and thermal thickness variation with arc-length, measured along the flame contour from $x = 0$ to the vortex-pair centerline, at $t = 0.16$ ms. Data is presented for each of the stiff (B) and nonstiff (A) schemes, overlaid on each other.

This flow field was also computed using the nonstiff scheme. A time step of 4 ns was chosen, larger than the above 2 ns dictated by chemical stiffness stability. As we shall see shortly, the overall flow features predicted by both schemes are nearly identical in the initial stages of the computation, and very similar for the entire simulation. However, with a time step that exceeds the threshold dictated by the stiffness of the reaction, the nonstiff scheme suffers from the growth of small-amplitude instabilities as would be expected. Nonstiff scheme computations with 2 ns time steps were prohibitively expensive, while those made using a 4 ns time step provided both useful early time results and a clear illustration of the onset of instability.

We start by noting that the global flow dynamics predicted by the nonstiff scheme are nearly identical to those shown in Fig. 3. In fact, the relative root-mean-square deviation between the two schemes, whether based on temperature, density, velocity, or overall heat-release rate, remains less than 0.2% during the entire period of the simulation $0 \leq t \leq 0.3$ ms. Further examination of the computations also leads to similar observations.

For instance, we plot in Fig. 4, for both stiff and nonstiff schemes, the variation of the local flame burning speed (displacement speed based on the unburnt reactants density, $S_d^u = \rho S_d / \rho_u$) and thermal thickness (based on the temperature rise across the flame and the peak local temperature gradient normal to the flame, $(T_b - T_u)/(\partial T/\partial n)_{\max}$). The figure shows both quantities plotted against flame arc-length, with an origin at the flame intersection with the left domain boundary and extending to the vertical centerline. Both identify clearly the location of the curved flame cusp. The flame thickness is seen to increase significantly at the cusp location, due to the local compressive tangential strain and the ensuing broadening of the flame structure. On the other hand, the thickness decreases in regions of large tangential stretch near the centerline. This dependence of the flame thickness on stretch has been noted in [61] and is a result of the convective strain field acting on the flame. Referring again to Fig. 4, the flame speed is found to be in the vicinity of 20 cm/s at the left domain boundary, decaying rapidly to a large negative value at the cusp and

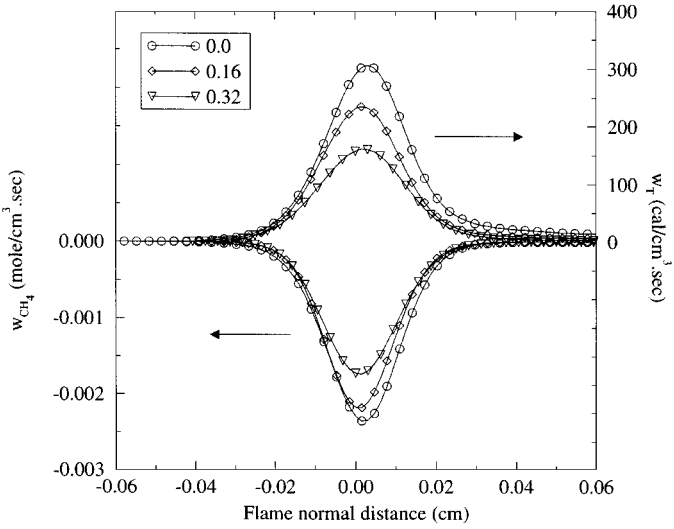


**FIG. 5.** A normal slice section of the flame at the vortex-pair centerline showing $CH_4$ consumption rate ($w_{CH_4}$) and flame heat release rate ($w_T$) profiles, using both stiff and nonstiff schemes, at times 0, 0.16, and 0.32 ms. The $x$-axis is the flame normal distance, measured from a reference point defined as the location where $Y_{CH_4}$ is 10% of $Y_{CH_4,\max}$. The results from both schemes are overlaid and are in such agreement that their differences are not discernible on the scale of the plot.

tending to a smaller, still negative value, at the centerline. Negative flame speeds have been observed in 1D flames using simple chemistry [61] and at positively curved cusps in a 2D turbulent premixed methane–air flame using detailed $C_1$ kinetics [62]. In [33], similar observations were evident using the above nonstiff scheme (with a stable time step) for the same vortex-pair interaction using a skeletal $C_1$ kinetic mechanism. The present computations using either of the two numerical schemes presented above give virtually identical results, as shown in Fig. 4. The maximum deviation observed in these profiles is 0.14%.

Agreement between the two schemes is also evident in normal flame slices at the centerline and at the cusp region for reaction source terms. As an example, consider the consumption rate of $CH_4$ and the heat release rate at both locations, shown in Figs. 5 and 6, respectively. In either case, consistent with earlier data [33], the fuel consumption rate and the heat release rate decay in time due to the interaction with the vortex pair. Here, again, the results from the two schemes are indistinguishable in the figures. The maximum deviation in these profiles on the centerline is 0.03%. At the cusp, the peak rms deviation at $t = 0.16$ ms is 0.03%, rising to 4.6% at $t = 0.32$ ms. The latter deviation may be traced to the sharpness of the cusp, and the corresponding error/noise in identifying the peak curvature location and the construction of the normal vector. Overall, however, the agreement between the two schemes is good both at the centerline and the cusp.

On the other hand, detailed inspection of the data reveals a growing wiggle in the nonstiff scheme results due to the large (4 ns) time step as expected. This problem is not evident in the stiff scheme results, which are computed with a stable time step. In order to illustrate this, consider the centerline slice of the net production rate of $CH_2^*$, a species with large (roughly equal and opposite) production and consumption rates, shown in Fig. 7. Here again, the global features allow no distinction between the profiles corresponding to each scheme.

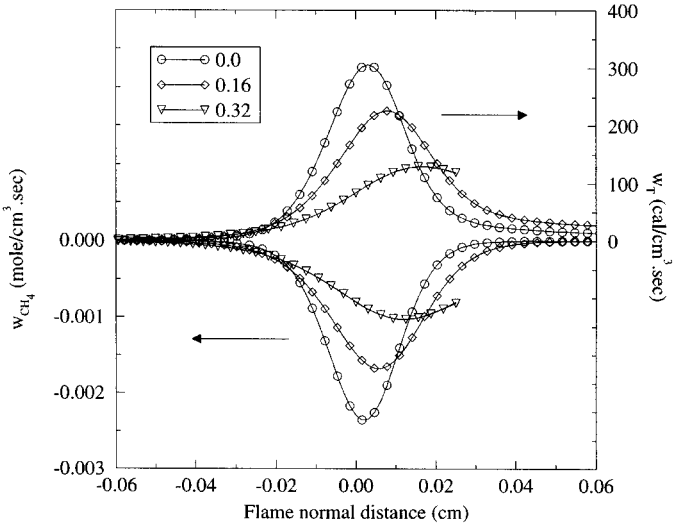


**FIG. 6.** A normal slice section of the flame at the curved cusp showing $CH_4$ consumption rate ($w_{CH_4}$) and flame heat release rate ($w_T$) profiles, using both stiff and nonstiff schemes, at times 0, 0.16, and 0.32 ms. The $x$-axis is the flame normal distance, measured from a reference point defined as the location where $Y_{CH_4}$ is 10% of $Y_{CH_4,max}$.

The plot shows the variation of $w_{CH_2^*}$ in time, and the A and B profiles are coincident at this resolution for all time. On the other hand, a small but growing anomaly is observed on the left-hand side of the figure. Looking more closely at this region, as shown in Fig. 8, a high-frequency growing wiggle is clearly evident in the nonstiff (A) scheme results with $\Delta t = 4$ ns, but nonexistent in the stiff (B) scheme results with $\Delta t = 20$ ns. For the present short-time simulation, the amplitude of this anomaly is still two orders of magnitude smaller

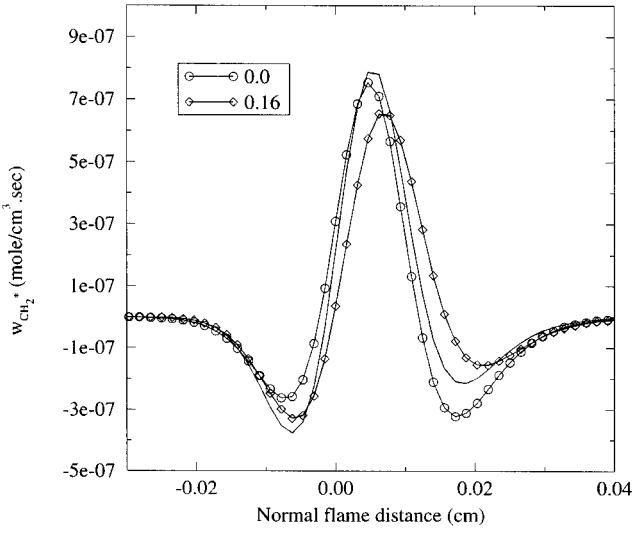


**FIG. 7.** A normal slice section of the flame at the vortex-pair centerline showing the $CH_2^*$ production rate ($w_{CH_2^*}$) profile, using both stiff and nonstiff schemes, at times 0, 0.16, and 0.32 ms. The $x$-axis is the flame normal distance, measured from a reference point defined as the location where $Y_{CH_4}$ is 10% if $Y_{CH_4,max}$.

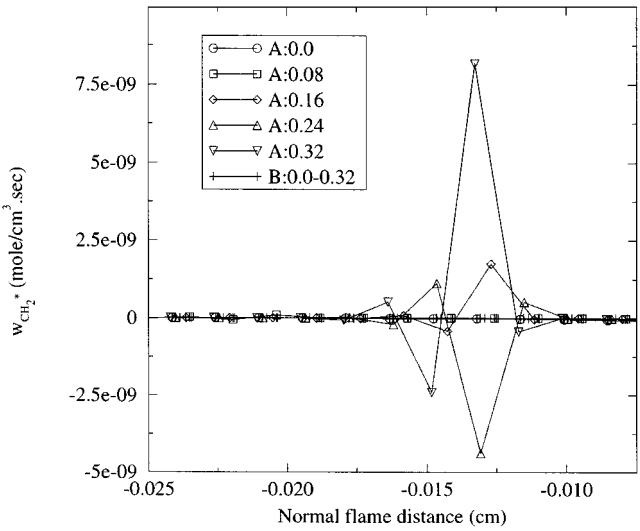


**FIG. 8.** An amplified portion of the the $CH_2^*$ production rate ($w_{CH_2^*}$) profile, on the reactants side of the flame, along the vortex-pair centerline. Data is plotted using both stiff (B) and nonstiff (A) schemes for several time instances from 0 to 0.32 ms, as indicated. The $x$-axis origin in this plot is shifted from that in Fig. 7.

than the peak $w_{CH_2^*}$ data. However, it is evident that for longer simulation times the nonstiff scheme requires a smaller time step, roughly less than 2 ns, to stabilize the predictor–corrector time integration. On the other hand, the stiff scheme continues to be stable at 20 ns.

Thus, the stiff scheme results are found to be stable, convergent, and consistent with available data in 2D unsteady reacting flow. With the above factor of 10 increase in the time step and given the additional computational overhead, the stiff scheme is found to be faster by a factor of 5 in 2D on available computational hardware. This is a substantial advantage that allows efficient computations of lean-to-rich methane flames with detailed kinetics in generic flows that involve unsteady 2D flame–flow interaction.

## 5. CONCLUSIONS

An efficient numerical scheme for the simulation of low-Mach-number reacting flow with detailed chemistry is developed. The construction is based on an extension of a predictor–corrector projection formulation for reacting flow with large density variation. The extension is based on modifying the corrector step by incorporating, in a nonsplit semi-implicit formulation, a stiff time-integration approach for the terms affected by the reaction source terms. The stiff integration code DVODE is adapted to this purpose.

The performance of the stiff scheme is analyzed empirically in one dimension, based on unsteady computations of a premixed methane–air flame, and in two dimensions through a detailed simulation of the interaction of the same flame with a counterrotating vortex pair. In all cases, the GRImech1.2 reaction mechanism, which involves 32 species and 177 elementary reactions, is used. Results of the stiff computations are compared to data obtained using the original nonstiff scheme with significantly smaller time steps. Unsteady one-dimensional computations indicate that the stiff scheme retains the second-order convergence properties of its predecessor. In addition, both 1D and 2D tests indicate that the

stiff scheme overcomes the time step restrictions associated with the stiffness of the reaction. For the presently considered reaction mechanism, the stiff scheme achieves speedup factors of about 10 in one dimension and roughly five in two dimensions.

It should be emphasized that the encouraging improvement exhibited by the stiff scheme is by no means immediate and is not achieved by simple incorporation of DVODE on any hardware. The speedup factors achieved are machine dependent [14]. The estimates provided here reflect experience on an SGI PowerChallenge-L with eight R10K processors and 1 MB secondary cache size. The present speedup has been reached following careful optimization of the reaction rate and Jacobian code structure on this hardware to minimize the overhead related to memory access. Moreover, the data-organization structure of DVODE had to be altered in order to allow local execution on shared-memory processors with no data dependencies.

The present computations reveal that, in its current version, the limitations of the stiff scheme are due to a somewhat severe diffusive time step restriction, which is dictated by the gas mixture properties and flame spatial scales. Future extension of this work will focus specifically on means to overcome this limitation and will also target further enhancement of the stiff solver. Ultimately, our aim is the development of an unsteady, multidimensional, low Mach number reacting flow solver which overcomes both the chemical and diffusive stiffness of the equations in an efficient, stable, and accurate fashion. In this ideal situation, selection of suitable integration time steps would be primarily governed by accuracy and resolution considerations only.

## ACKNOWLEDGMENT

This work was supported by the U.S. Department of Energy (DOE), the DOE Office of Basic Energy Sciences, Chemical Sciences Division, and the DOE Defense Programs Accelerated Strategic Computing Initiative (ASCI). Computational support was provided by the DOE National Energy Research Supercomputer Center (NERSC). The authors would like to thank Dr. Joseph Grcar for many helpful discussions.

## REFERENCES

1. R. Aiken (Ed.), *Stiff Computation* (Oxford Univ. Press, Oxford, 1985).
2. E. Hairer and G. Wanner, *Solving Ordinary Differential Equations II, Stiff and Differential-Algebraic Problems* (Springer-Verlag, Berlin, 1996).
3. C. F. Curtiss and J. O. Hirschfelder, Integration of stiff equations, *Proc. Nat. Acad. Sci.* **38**, 235 (1952).
4. C. W. Gear, *Numerical Initial Value Problems in Ordinary Differential Equations* (Prentice–Hall, Englewood Cliffs, NJ, 1971).
5. A. C. Hindmarsh, Technical Report UCID-30001, Rev. 3, Lawrence Livermore National Laboratory, Livermore, CA, 1974.
6. A. C. Hindmarsh, Technical Report UCID-30059, Rev. 2, Lawrence Livermore National Laboratory, Livermore, CA, 1977.
7. A. C. Hindmarsh, LSODE and LSODI, two new initial value ordinary equation solvers, *ACM-SIGNUM* **15**(4), 10 (1980).
8. A. C. Hindmarsh, in *Scientific Computing*, edited by R. Stepleman (North-Holland, Amsterdam, 1983), p. 55.
9. P. N. Brown, G. D. Byrne, and A. C. Hindmarsh, VODE: A variable coefficient ODE solver, *SIAM J. Sci. Stat. Comput.* **10**, 1038 (1989).

10. H. H. Robertson, in *Numerical Analysis, An Introduction*, edited by J. Walsh (Academic Press, 1966), p. 178.
11. R. D. Saylor and G. D. Ford, On the comparison of numerical methods for the integration of kinetic equations in atmospheric chemistry and transport models, *Atmos. Environ.* **29**(19), 2585 (1995).
12. J. G. Verwer and M. van Loon, An evaluation of explicit pseudo-steady-state approximation schemes for stiff ODE systems from chemical kinetics, *J. Comput. Phys.* **113**, 347 (1994).
13. K. Radhakrishnan, New integration techniques for chemical kinetic rate equations. I. Efficiency comparison, *Combust. Sci. Technol.* **46**, 59 (1986).
14. Y. D'Angelo and B. Larrouturou, Comparison and analysis of some numerical schemes for stiff complex chemistry problem, *RAIRO. Math. Model. and Numer. Anal.* **29**, 259 (1995).
15. J. G. Verwer, Gauss-Seidel iteration for stiff ODES from chemical kinetics, *SIAM J. Sci. Comput.* **15**, 1234 (1994).
16. J. G. Verwer, J. G. Blom, and E. J. Spee, A comparison of stiff ODE solvers for atmospheric chemistry problems, *Atmos. Environ.* **30**, 49 (1996).
17. C. J. Aro, CHEMSODE: A stiff ODE solver for the equations of chemical kinetics, *Comput. Phys. Commun.* **97**, 304 (1996).
18. Baeza, J. J. Baeza, Plá, F. Pérez, and Ramos, G. Ramis, Stiffness-adaptive taylor method for the integration of non-stiff and stiff kinetic models, *J. Comput. Chem.* **13**, 810 (1992).
19. P. Sun, D. P. Chock, and S. L. Winkler, An implicit-explicit hybrid solver for a system of stiff kinetic equations, *J. Comput. Phys.* **115**, 515 (1994).
20. D. P. Chock, S. L. Winkler, and P. Sun, Comparison of stiff chemistry solvers for air quality modeling, *Environ. Sci. Technol.* **28**, 1882 (1994).
21. D. Dabdub and J. H. Seinfeld, Extrapolation techniques used in the solution of stiff ODEs associated with chemical kinetics of air quality models, *Atmos. Environ.* **29**, 403 (1995).
22. S. Elliot, R. P. Turco, and M. Z. Jacobson, Tests on combined projection/forward differencing integration for stiff photochemical family systems at long time step, *Comput. Chem.* **17**, 91 (1993).
23. E. Hesstvedt, O. Hov, and I. S. A. Isaksen, Quasi-steady-state approximations in air pollution modeling: Comparison of two numerical schemes for oxidant prediction, *Int. J. Chem. Kinetics* **10**, 971 (1978).
24. T. R. Young and J. P. Boris, A numerical technique for solving stiff ordinary differential equations associated with the chemical kinetics of reactive flow problems, *J. Phys. Chem.* **81**, 2424 (1977).
25. W. Gong and H.-R. Cho, A numerical scheme for the integration of the gas-phase chemical rate equations in three-dimensional atmospheric models, *Atmos. Environ.* **27A**, 2591 (1993).
26. K. Radhakrishnan, Integrating combustion kinetic rate equations by selective use of stiff and nonstiff methods, *AIAA J.* **25**, 1449 (1987).
27. G. Goyal, P. J. Paul, H. S. Mukunda, and S. M. Deshpande, Time dependent operator-split and unsplit schemes for one dimensional premixed flames, *Combust. Sci. Tech.* **60**, 167 (1988).
28. X. Zhong, Additive semi-implicit Runge–Kutta methods for computing high-speed nonequilibrium reactive flows, *J. Comput. Phys.* **128**, 19 (1996).
29. U. Mass and S. B. Pope, *Twenty-Fourth Symposium (International) on Combustion, The Combustion Institute, 1992*, p. 103.
30. S. Mahalingam, B. J. Cantwell, and J. H. Ferziger, Report TF-43, Thermosciences Division, Dept. of Mechanical Engineering, Stanford University, Stanford, CA, 1989.
31. E. S. Oran, in *Computational Fluid Dynamics and Reacting Gas Flows*, edited by A. M. M. Luskin and B. Engquist (Springer-Verlag, New York, 1988), p. 291.
32. V. R. Katta, L. P. Goss, and W. M. Roquemore, Numerical investigations of transitional $H_2/N_2$ jet diffusion flames, *AIAA J.* **32**(1), 84 (1994).
33. H. N. Najm and P. S. Wyckoff, Premixed flame response to unsteady strain-rate and curvature, *Combust. Flame* **110**(1–2), 92 (1997).
34. H. N. Najm, in *Transport Phenomena in Combustion*, edited by S. Chan (volume 2, Taylor & Francis, Washington, DC, 1996), p. 921.

35. A. Majda and J. Sethian, The derivation and numerical solution of the equations for zero mach number combustion, *Combust. Sci. and Technol.* **42**, 185 (1985).
36. A. F. Ghoniem and O. M. Knio, *Twenty-First Symposium (International) on Combustion, The Combustion Institute, 1986*, p. 1313.
37. O. M. Knio, A. S. Worlikar, and H. N. Najm, *Twenty-Sixth Symposium (International) on Combustion, The Combustion Institute, 1996*, p. 203.
38. H. Schlichting, *Boundary-Layer Theory*, 7th ed. (McGraw–Hill, New York, 1979).
39. F. A. Williams, *Combustion Theory*, 2nd ed. (Addison–Wesley, New York, 1985).
40. R. J. Kee, F. M. Rupley, and J. A. Miller, Sandia Report SAND89-8009B, Sandia National Labs., Livermore, CA, 1993.
41. A. J. Chorin, A numerical method for solving incompressible viscous flow problems, *J. Comput. Phys.* **2**, 12 (1967).
42. J. Kim and P. Moin, Application of a fractional-step method to incompressible Navier–Stokes equations, *J. Comput. Phys.* **59**, 308 (1985).
43. P. A. McMurtry, W.-H. Jou, J. J. Riley, and R. W. Metcalfe, Direct numerical simulations of a reacting mixing layer with chemical heat release, *AIAA J.* **24**(6), 962 (1986).
44. S. Mahalingam, B. J. Cantwell, and J. H. Ferziger, Full numerical simulations of coflowing, axisymmetric jet diffusion flames, *Physics of Fluids A*, **2**, 720 (1990).
45. D. A. Anderson, J. C. Tannehill, and R. H. Pletcher, *Computational Fluid Mechanics and Heat Transfer* (Hemisphere Pub. Co., New York, 1984).
46. C. Rutland, J. H. Ferziger, and B. J. Cantwell, Report TF-44, Thermosciences Div., Mech. Eng., Stanford Univ., Stanford, CA, 1989.
47. C. J. Rutland and J. H. Ferziger, Simulations of flame-vortex interactions, *Combust. Flame* **84**, 343 (1991).
48. M. Frenklach, H. Wang, M. Goldenberg, G. P. Smith, D. M. Golden, C. T. Bowman, R. K. Hanson, W. C. Gardiner, and V. Lissianski, Topical Report GRI-95/0058, Gas Research Institute, 1995.
49. R. J. Kee, J. F. Grcar, M. D. Smooke, and J. A. Miller, Sandia Report SAND85-8240, Sandia National Labs., Livermore, CA, 1993.
50. W. T. Ashurst and P. A. McMurtry, Flame generation of vorticity: Vortex dipoles from monopoles, *Combust. Sci. and Technol.* **66**, 17 (1989).
51. T. Poinsot, D. Veynante, and S. Candel, Quenching processes and premixed turbulent combustion diagrams, *J. Fluid Mech.* **228**, 561 (1991).
52. T. Mantel, Annual research briefs, Center for Turbulence Research, Stanford University/NASA Ames Research Center, (1994).
53. M. Hilka, D. Veynante, M. Baum, and T. J. Poinsot, *Tenth Symp. on Turbulent Shear Flows*, volume 2, University Park, PA, (1995), *Penn. State Univ.*, p. 19.
54. J. Jarosinski, J. H. Lee, and R. Knystautas, *Twenty-Second Symposium (International) on Combustion, The Combustion Institute, 1988*, p. 505.
55. W. L. Roberts, J. F. Driscoll, M. C. Drake, and L. P. Goss, Images of the quenching of a flame by a vortex-to quantify regimes of turbulent combustion, *Combust. Flame* **94**, 58 (1993).
56. J.-M. Samaniego, Annual research briefs, Center for Turbulence Research, Stanford University/NASA Ames Research Center, (1993).
57. C. J. Mueller, J. F. Driscoll, D. J. Sutkus, W. L. Roberts, M. C. Drake, and M. D. Smooke, Effect of unsteady stretch rate on OH chemistry during a flame-vortex interaction: To assess flamelet models, *Combust. Flame* **100**, 323 (1995).
58. Q.-V. Nguyen and P. H. Paul, *Twenty-Sixth Symposium (International) on Combustion, The Combustion Institute, 1996*, p. 357.
59. C. J. Mueller, J. F. Driscoll, D. L. Reuss, M. C. Drake, and M. E. Rosalik, Vorticity generation and attenuation as vortices convect through a premixed flame, *Combust. Flame* **112**, 342 (1998).

60. N. Peters, in *Turbulent Reactive Flows*, edited by R. Borghi and S. Murthy (Springer-Verlag, New York, 1989), p. 242.
61. N. Darabiha, S. M. Candel, and F. E. Marble, The effect of strain rate on a premixed laminar flame, *Combust. Flame* **64**, 203 (1986).
62. I. Gran, T. Echekki, and J. H. Chen, *Twenty-Sixth Symposium (International) on Combustion, The Combustion Institute, 1996*, p. 323.